Fuel 274 (2020) 117856

Contents lists available at ScienceDirect

Fuel

journal homepage: www.elsevier.com/locate/fuel

Aging brine-dependent deposition of crude oil components onto mica substrates, and its consequences for wettability

M.E.J. Haagh[a], N. Schilderink[a], M.H.G. Duits[a,*], I. Siretanu[a], P. Krawiec[b], I.R. Collins[b], F. Mugele[a]

[a] Physics of Complex Fluids Group and MESA Institute, Faculty of Science and Technology, University of Twente, PO Box 217, 7500 AE Enschede, The Netherlands
[b] BP Exploration Operating Company Limited, Chertsey Road, Sunbury on Thames, Middlesex TW16 7LN, UK

GRAPHICAL ABSTRACT

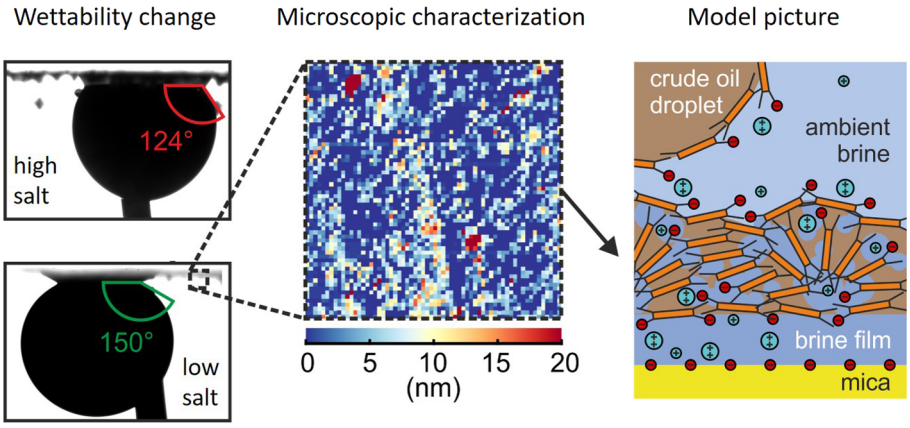

ARTICLE INFO

Keywords:
Enhanced oil recovery
Low salinity water flooding
Contact angle
Aging
Adsorption
Asphaltenes

ABSTRACT

While wettability alteration is widely accepted as the dominant mechanism underlying enhanced oil recovery (EOR) in sandstone reservoirs under low salinity water flooding (LSWF) conditions, the effectiveness of LSWF still varies substantially between laboratory experiments and the field indicating our incomplete understanding and control of the process. We use simple mica substrates to investigate the impact of aging conditions on the macroscopic contact angle and the microscopic properties (morphology, composition, stiffness, surface charge) of the surface. Mica samples pre-aged in brines of variable salt content prior to aging in crude oil at elevated temperature displayed macroscopic wettabilities ranging from complete water wetting to intermediate contact angles around 90° in ambient brines of variable salinity. Compared to the macroscopic wettability, variations of the microscopic properties as probed by Atomic Force Microscopy and Confocal Raman microscopy were found to be rather subtle. Clear signatures of asphaltenic deposits were observed ubiquitously, usually consisting of a combination of a thin film and larger aggregates. The deposits typically displayed a salinity-dependent elasticity and (predominantly negative) surface charge. Selective removal of ions from the pre-aging brine lead to strong variations of both macroscopic wettability and microscopic properties, including the response to low ambient salinity: For the same crude oil, reducing the salinity of the ambient brine can either increase or decrease the

Abbreviations: AFM, Atomic Force Microscopy; ARCA, Advancing and Receding Contact Angle; ASW, Artificial Sea Water; CRM, Confocal Raman Microscopy; EMCCD, Electron Multiplying Charge Coupled Device; EOR, Enhanced Oil Recovery; LSWF, Low Salinity Water Flooding; MIE, Multi-component Ion Exchange; SARA, Saturate Aromatic Resin Asphaltene; SEM, Scanning Electron Microscopy; TAN, Total Acid Number

* Corresponding author.
E-mail address: M.H.G.Duits@utwente.nl (M.H.G. Duits).

https://doi.org/10.1016/j.fuel.2020.117856
Received 9 January 2020; Received in revised form 16 March 2020; Accepted 12 April 2020
Available online 18 April 2020

macroscopic oil contact angle, depending on the composition of the formation brine used to pre-age the mineral surface. These results clearly highlight the complex balance of interactions during brine-oil-rock aging and the subtle role of the connate water composition in extracting and binding different types of crude oil components and thereby setting the initial and boundary conditions for the oil recovery process.

1. Introduction

The global average recovery factor from mature oil fields by conventional water flooding is somewhere between 20% and 40% [1]. Enhanced oil recovery (EOR) techniques are employed in order to extract some of the remaining, 'trapped' oil. Low Salinity Water Flooding (LSWF) is an attractive EOR method that can improve the microscopic water-oil displacement efficiency by more than 20% in favorable cases. It is nowadays widely believed that this increase is caused by an improved water-wettability in mixed-wet sandstone reservoirs upon salinity reduction [2,3]. Wettability is generally considered as a macroscopic property that can be quantified by contact angle measurements on the millimeter scales, as we will do in this work. Yet, the origin of the macroscopic contact angle lies in the molecular interactions between rock, brine, and crude oil including all its components on the nanometer length scale [3–5]. It is by shifting the subtle balance these interactions that LSWF can alter the macroscopic wettability of the system. Low salinity brine is typically only the last of a row different types of brines that interact with the rock throughout the lifetime of a reservoir from its diagenesis to the final stages of production. Initially, connate brine, rock, and crude oil together generate the typically mixed-wet initial state of the system as polar components from the crude oil adsorb onto the rock on geological time scales. Subsequently, seawater is injected in secondary mode and LSW is typically only injected in the final tertiary recovery phase. It has been conjectured that the injected brines do not interact with the rock directly, but instead with the thin organic layer strongly bound to it that has formed upon aging [6]. LSWF is then thought to reduce the salinity-dependent attractive interactions between the organic components and the rock and thereby turn the rock more hydrophilic again [7]. Mechanistically, it is believed that this reduction of attraction is caused by primarily by multiple-ion-exchange, pH increase, electric double layer expansion, or a combination of these effects.

Notwithstanding an increasing consensus in the field favoring the just mentioned mechanisms, experimental results are still highly variable and the predictive power of existing models is rather poor, suggesting a lack of true fundamental insight [8]. Probably, this failure has to be attributed to a combination of effects related to both variations in the composition of the fluids involved and variations of experimental procedures. An important aspect of the experimental procedures is the aging of the rock surface to reinstate conditions at the beginning of the laboratory experiment that mimic the initial conditions encountered in the reservoir. Aging protocols typically involve first exposure of the rock to a formation (or connate) brine and subsequently exposure of the rock to crude oil. While it is well-known that the initial aging in brine is crucial for the observation of enhanced recovery upon LSWF, systematic studies of the impact of the aging brine composition on crude oil aging and the subsequent wettability state of sandstone rock are remarkably sparse. Sharma and Filoco reported that the salinity of the connate water was the primary factor controlling oil recovery [9]. Liu et al. showed that an aging step with Mg^{2+} ions in combination with ionized organic acids in crude oil and negatively charged sand surfaces can change the wettability of a heavy oil/brine/sand system [10]. Yang et al. found similar effects, but studied only the impact of the Ca^{2+} ion concentration in the connate water [11]. Shehata and Nasr-El-Din showed that LSWF recovery was higher if the concentration of divalent cations (Ca^{2+} and Mg^{2+}) was increased in the connate water [12], presumably because of wettability differences induced by the increasing ion concentration. However, no systematic variation of the ionic composition was performed. A major difficulty contributing to the lack of systematic studies is certainly the fact that core flood experiments are time-consuming and costly. This compromises the ability to perform 'high-throughput' screening for optimized LSWF recipes. Moreover, it is notoriously difficult to access the interior of core samples for microscopic in situ characterization of structure and composition [13], typically requiring mechanical slicing or FIB (focused ion beam) dissection. Measurements of microscopic contact angles in porous media have recently become possible (e.g. in x-ray tomography) [14,15], yet such measurements require specific fluid compositions that deviate from the complex fluids in EOR.

In the present work, we study systematically the influence of the composition of the aging brine on the macroscopic contact angle of flat mica substrates representing a sandstone like mineral surface. While circumventing in this manner the complexity arising from the three-dimensional pore structure, this approach allows us to retain the relevant surface chemistry [3,4,16,17] while gaining access with a suite of surface characterization techniques including various manners of atomic force microscopy (AFM) imaging and spectroscopy, confocal Raman microscopy (CRM) and scanning electron microscopy (SEM). The mica slides are initially aged in connate brines of variable composition followed by aging in crude oil at elevated temperature. Subsequent measurements of advancing oil contact angles in ambient brines of variable salinity demonstrate a significant effect of the composition of the initial aging brine on the wettability of various crude oils in 'measurement' brines of variable salinity. To rationalize our macroscopic observations, we characterize the topography and chemical composition of the samples after aging in crude oil using AFM and CRM in ambient air. These measurements clearly reveal the presence of organic deposits on the mica surfaces. Yet, despite significant variations of the macroscopic wettability, the surface composition and topography

Table 1
Ion concentrations, ionic strength, calculated Debye length, and measured pH of all the main brines used in this work (see Supplementary Table S2 for a complete overview). Sample codes with a dash indicate depletion of a specific species (-c for bicarbonate, and $-M^{2+}$ for divalent cations).

	Brine name	*Ion concentration (mM)*						*IS* (mM)	*λD* (nm)	*pH*
		Na^+	K^+	Ca^{2+}	Mg^{2+}	Cl^-	HCO_3^-			
High salinity	ASW	404	10	13	112	660	2.3	792	0.3	8.8
	ASW-c	402	10	13	112	660	0	786	0.3	6.0
	ASW-M^{2+}	404	10	0	0	410	2.3	417	0.5	8.7
	CBA	990	10	119	21	1280	0	1420	0.3	5.7
Low salinity	lsASW	13	0	0	4	21	0.1	25	1.9	8.7
	lsCBA	14	0	2	0	17	0	20	2.2	6.3

display a remarkably weak response to systematic modifications of the aging brines such as depletion of divalent cations, bicarbonate ions and changes in temperature and pH. In situ AFM spectroscopy in variable brine reveals changes of the local surface charge and elasticity for certain conditions.

2. Experimental

Four different types of crude oil (designated as A, B, C and D) were obtained from BP, Sunbury (UK). Acid and base number, saturated, aromatic, resin and asphaltene (SARA) contents are specified in Supplementary Table S1. As solid substrate we used sheets of muscovite mica (B & M Mica Co., Inc.). All other chemicals were reagent grade and purchased from Sigma. Brine phases (see Table 1 for the most commonly discussed brines in this paper, and Supplementary Table S2 for an overview of all brines used in this work) were prepared by dissolving combinations of inorganic salts in deionized water (Millipore, resistivity 18.2 MΩcm). A distinction is made between artificial connate brines (CB) and artificial sea water (ASW), where CBs mimic reservoir aging conditions, and (modifications of) ASW correspond to seawater-based compositions. The pH of the brines was adjusted at room temperature by adding small amounts of 0.1 M NaOH or HCl.

The brines and crude oils used for aging were pipetted into glass vials and kept in an oven at 60 °C unless indicated otherwise. Mica slides were cleaved in air and immediately immersed in the aging brine for 24 h. After removal from the aging brine, the mica sheets were held vertically in the air and excess fluid was allowed to drain for ≈1 min. Before the samples dried out they were immersed in crude oil and placed back into the oven, where they were left to age for another 4 days at 60 °C. Subsequently, the samples were allowed to cool down for 30 min, removed from the crude oil and rinsed with toluene to remove all excess crude oil that was not strongly bound to the surface. This process produces a thin transparent organic film on top of the mica sheets. Finally, the samples were blown dry with nitrogen and stored under nitrogen atmosphere.

Contact angle measurements were performed with the mica slide attached to a quartz substrate and immersed horizontally in the measurement brine at 60 °C. A curved needle with oil was then inserted in the brine phase and allowed to thermally equilibrate with the ambient brine for 1 min before generating a 30 μL oil droplet. The drop was brought in contact with the sample and the volume was increased and decreased, each over a period of 40 min (see Fig. 1). Advancing and receding contact angle (ARCA) measurements were performed on a Dataphysics OCA 20L goniometer equipped with a droplet dispensing unit, a temperature control stage (Dataphysics TFC 100Pro) and SCA20 Analysis Software. A home-made copper casing with a window for the optical path was mounted around the cuvette, and a thermometer in the brine was used to ensure the set temperature. Oil injection and retraction were carried out slowly because of the high oil viscosities. For each condition (aging brine, crude oil, ambient brine) 5–6 ARCA measurement series were done, with 2 measurements per sample.

AFM imaging of dried substrates was performed using amplitude modulation (20 nm amplitude, set point at 18 nm) in air using NSC36 cantilevers (MikroMasch) in a Bruker Dimension Icon. Height maps h (x,y) of these samples were analyzed for roughness and for the fractional coverage by protrusions. Here the RMS roughness is calculated (similar to Ref. [18]) as the square root of the variance of all heights (where each (x,y) image pixel provides 1 height measurement). Protrusions were identified as those pixels where $\Delta h > 10$ nm relative to the lowest measured h.

We also performed force volume measurements in ambient brine, using Scanasyst-Fluid cantilevers (Bruker), at room temperature. For the measurements in ambient brine, the substrates (aged in ASW, ASW-c, and ASW-M^{2+}) were placed in a glass petri dish and submerged together in 10 ml brine. Forces were measured subsequently in ASW, lsASW, and finally in 1 mM NaCl. The pH of these fluids was set to 6 by adding HCl to ensure a constant pH through the duration of the measurements (≈8 h). Upon switching from one brine to another, the fluid in the measurement cell was exchanged three times while keeping the samples submerged. The latter allowed us to use the same AFM tip and substrate for several measurement conditions. For the force volume measurements, approach and retract curves were recorded on a grid of 100 × 100 or 64 × 64 pixels with a maximum force upon closest approach of 5 nN. *F(z)*, force versus piezo displacement, curves were converted into *F(d)*, force vs. tip-sample separation, curves using standard procedures, see Supplementary Fig. S1. Assuming that the indentation regime can be described by a force model where the cantilever and the substrate are two Hookean springs in series, the stiffness ('spring constant') of the substrate is extracted.

The surface charge densities for each substrate in each of the different brines were calculated by fitting an electrostatic interaction model to the long-range ($d > 5$ nm) part of the *F(d)* approach curve. Experimental procedures and data analysis follow the principles described in references [18,19]. A simplified standard model was used to describe the interaction between two asymmetrically charged surfaces, the silica tip and the aged mica substrate, for weak overlap of the electric double layers [20]:

$$F(d) = \frac{2\pi r^2 \sigma_{tip}\sigma_{sample}}{\varepsilon_0 \varepsilon} e^{-\frac{d}{\lambda_D}} \quad (1)$$

Here, r is the interaction radius, σ_i is the charge density of surface i (σ_{sample} was used as a fit parameter, while σ_{tip} was extracted from a separate calibration measurement on a clean silica sample and was kept constant during fitting at -0.08 e/nm^2 [19]. $\varepsilon_0\varepsilon$ is the dielectric constant of water, and λ_D, the Debye screening length, was also used as a fit parameter. The tip-sample interaction radius was estimated to be 16 nm (corresponding well to the 20 nm tip radius given by the manufacturer) by fitting the function to a reference measurement on a silica substrate. In addition, it assumes that the tip geometry can be represented by a flat disk parallel to the surface. While the absolute values of the extracted surface charge densities are subject to errors due to the uncertainties and approximations involved in these calibration procedures, relative comparisons of σ_{sample} between different samples are reliable because compared measurements were all performed with the same AFM tip.

Raman images of aged mica substrates were obtained in air using a WiTec alpha 300R Raman microscope, connected to a 532 nm laser via an optical fiber, the entrance of which acted as a pinhole. A 600 g/mm grating was used, providing a spectral resolution of around 2.5 cm^{-1}. An EMCCD camera (1600 × 200 pixels, 16 μm pixel size, Andor Newton) was used for detection. For high spatial resolution, a 100 × objective (Zeiss, NA = 0.9) was chosen. The laser power was measured at the sample using an optical power meter (ThorLabs). The integration time was 400 ms/pixel. Intensity maps for asphaltene compounds are obtained by integrating the area under the peaks at 1350 and 1580 cm^{-1} for every pixel (see Fig. 6). The baseline was subtracted using an algorithm developed by Zhang et al. [21].

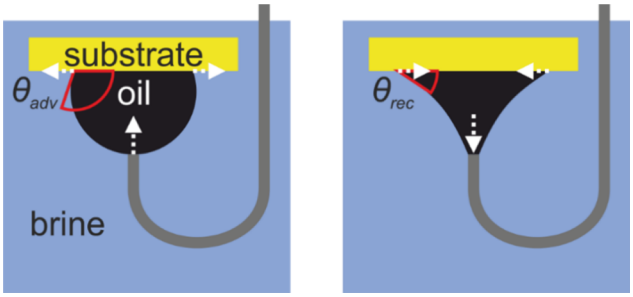

Fig. 1. Captive droplet ARCA set-up schematic. Advancing and receding angles of a crude oil droplet are measured on an aged mica slide, immersed in either high or low salinity brine at a set temperature of 60 °C.

3. Results

3.1. Macroscopic characterization

The wettability of the aged mica substrates was examined by ARCA measurements using oil droplets, as illustrated in Fig. 2A. This typical experiment shows that after ≈10 min of gradual inflation, the oil contact angle becomes fairly constant, while the base diameter is still increasing. The oil advancing contact angle, reflecting the most water-wet signature of the substrate, is thus measurable. The large angle of ≈140° indicates that the oil drop has to overcome strongly hydrophilic regions on the substrate. We note that these regions might consist of rather small 'wetting defects' such as spots of bare mica on the otherwise organic layer-covered substrate. Reference measurements on a bare mica substrate indeed showed that the crude oil does not wet this substrate. Upon deflating the droplet, the contact angle keeps decreasing for the majority of samples while the contact line remains pinned. A true receding contact angle is not reached in these cases, which is indicative of a very strongly oil-wet configuration. This ARCA signature with a strong contact angle hysteresis and very small receding contact angle was observed in most cases. Fig. 2B shows an exception to this picture, by displaying a finite receding c.a. of ≈90° for case of crude oil D primed and characterized in ambient ASW. For a few other conditions, complete water wetting was observed (even on the crude oil-aged samples) with both advancing and receding contact angles close to 180°, indicating the presence of a stable water layer between the substrate and the oil. For each specific material composition and aging condition the experiment was highly reproducible, as indicated by the error bars in Fig. 4. Occasional tests with samples that were aged for additional days in crude oil under the same conditions did not show any further evolution of the measured contact angles.

Fig. 3 shows a comparison of advancing contact angles of crude oil A measured in high and low salinity brines on mica slides aged in the same crude oil but primed with variable aging brine. The snapshots clearly show the intriguing result that lowering the ambient salinity can result in both higher and lower contact angles (for the same crude oil and the same ambient measurement brine), depending on the composition, in this case the pH, of the aging brine. Specifically, the aging brine had a pH of 8.8 in the middle row and pH 6.0 (typical for injected seawater in sandstone reservoirs) [22] in the bottom row. Apparently the aging brine, which plays the role of the connate brine, affects the low salinity response observed in later stages of the experiment.

This strikingly strong dependence on the aging brine is not limited to the pH but is also observed upon changing the ion content of the aging brine, as shown in Fig. 4. Clearly, the variation of the advancing θ_{oil} is very wide, and includes situations of complete water wetting if the divalent cations are removed from the aging brine (ASW-M^{2+}). The latter case implies that the crude oil drop remains separated from the aged mica surface by a thin but stable brine film. From the perspective of macroscopic phenomenology, the brine film gives rise to the same wetting behavior as freshly cleaved (i.e. non-aged) mica. Yet, as we will see in the AFM images below, the two types of surfaces are microscopically very different. Fig. S2 shows a more extended set of contact angle data for various crude oils, aging and measurement brine compositions. From that overview, it becomes clear that that the strong dependence (of both the contact angles and the low salinity effect) on details of the aging brine composition should indeed be regarded as a rather general phenomenon.

3.2. Ex-Situ AFM topography

Aiming for a better understanding of the origin of these macroscopic phenomena, we proceeded to characterize the samples microscopically using tapping mode AFM. To this end, we dried the toluene-washed mica samples after the completion of the aging steps and imaged them in air. Optical inspection reveals occasional defects on the sub-millimeter scale but displays otherwise a rather homogeneous coating with apparently well-defined average properties. Fig. 5 provides an overview of the surface topography over several length scales recorded in these representative areas of mica surfaces aged in crude oil A after priming in variable aging brine as indicated. For each aging condition we captured at least two images per scan range, obtained from different substrates, and consistently found rather similar looking structures. Fig. S3 shows similar data for other crude oils and aging conditions.

Despite the substantial variations of the response seen in the macroscopic contact angle, the surfaces look rather similar in AFM. All samples clearly display material that was deposited on the originally atomically flat mica surfaces during the aging procedure. The resulting surface roughness displays two characteristic length scales. Firstly there is a small-scale roughness with a typical lateral scale of several tens of nanometers and a rather uniform height of several nanometers (the surface is covered rather homogeneously). This structure is reminiscent of earlier reports studying crude oil treated substrates. Some authors attributed these features to micelles or aggregates of asphaltenes [23,24]. Secondly, on top of this layer, additional protrusions with a lateral size of a few micrometers and a wide range of heights of the order of 100 nm can be seen. Figs. S3 and S4 provide an overview of the root-mean-square roughness and the average coverage of the larger protrusions for the AFM images of Figs. 5 and S2. Notwithstanding the observed variations, no clear correlation between the topographic features of the surface and the macroscopic wettability could be identified. Only for crude oils C and D, the small-scale asphaltene aggregates seemed distinctly less prominent (Fig. S3). These oils are relatively low in asphaltene content (see Table S1).

3.3. Ex-situ confocal Raman microscopy

Complementary information about the dry samples was obtained using CRM. While this technique is in principle capable of unraveling

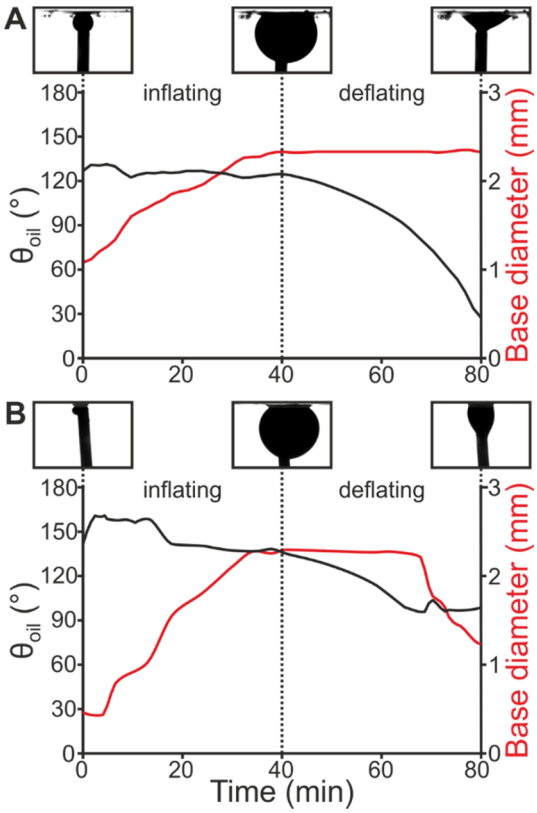

Fig. 2. Example ARCA measurements showing two types of behavior: commonly, A) an advancing-, but no receding contact angle (crude oil A, aged and measured in ASW), and rarely, B) both advancing- and receding contact angles (crude oil D, aged with ASW, pH 6, measured in ASW). All aging and measurements performed with mica, at 60 °C; contact angles measured in the oil phase.

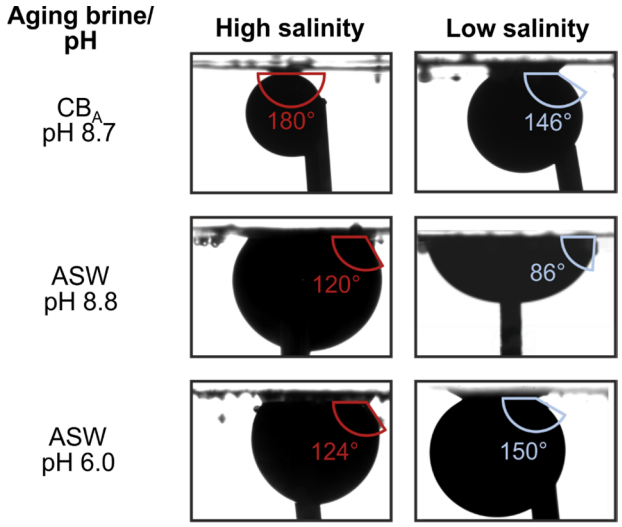

Fig. 3. Illustration of advancing contact angles of crude oil A on aged mica slides for T = 60 °C upon both aging and measurement. Top row: brines CB_A (left) and $lsCB_A$ (right). Middle and bottom rows: ASW and lsASW.

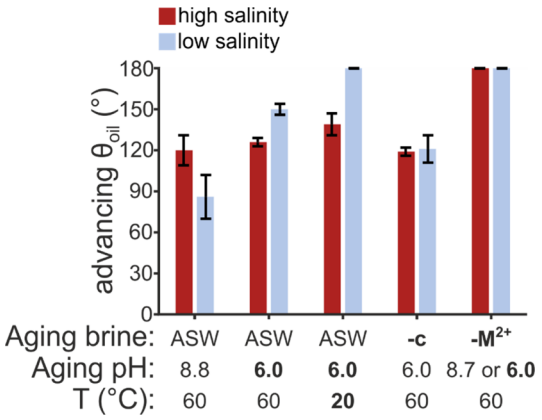

Fig. 4. Advancing contact angles of crude oil drops on mica, measured in ambient brines of high- and low-salinity ASW (pH ≈8.8, 60 °C). The difference between the data sets lies in the aging brines, which were all based on ASW (pH ≈8.8, 60 °C), but with different pH, temperature or the depletion of certain ions. These deviations from standard ASW are emphasized in boldface. Error bars indicate standard deviations of advancing contact angles.

the chemical make-up of structures observed through a light microscope based on the specific vibrational fingerprint of each molecule, the material adsorbed from the various crude oils onto the mica substrates displays a very strong background fluorescence that overwhelms much of the vibrational information. To proceed, we first de-noised the CRM spectra using principal component analysis (see reference for a recent discussion) [25] and subsequently removed the fluorescent background as shown in Fig. 6. After this procedure, the well-known peaks of the G-(1580 cm^{-1}) and D-(1350 cm^{-1}) bands associated with graphitic sheets are clearly visible and can be described by a superposition of four Gaussians. These peaks are known to be found in the presence of asphaltenes. They are attributed to their graphitic sheet-like structure and the defects such as broken bonds and substituted atoms therein [26].

Comparing the Raman and AFM topography maps taken at the same location on differently aged mica slides, we find a clear correspondence between topographic protrusions in the AFM maps and enhanced Raman scattering intensities in the range of the G- & D-bands (see Fig. 7). This supports the notion that the structures observed in the AFM images contain asphaltenes. We also find slight differences in the D- and G-band intensities, both between samples of different aging conditions, and within each sample when comparing the spectra from protrusions to the ones from films, see Fig. 7C. The spectra shown in this figure are consolidated from approximately 50.000 curves. This large number implies that the spectral differences, even though relatively subtle, are statistically relevant. They thus indicate significant chemical differences between the samples. For instance, slight differences in the intensity peak ratios between the D and G bands in Fig. 7C suggest that the average size of the asphaltenic aggregates in the protrusions is somewhat larger than in the adjacent film.

Remarkably, no evidence was found for a clear correlation between the microscopic structure and the macroscopic wettability. From Fig. 4, we know that the samples in the left and in the middle column of Fig. 7 display partial wetting, whereas the one aged in ASW-M^{2+} brine displays complete water wetting. Clearly, the modest differences between the microscopic images do not offer a basis for understanding the dramatic variations in contact angle.

3.4. *In situ AFM characterization*

A major difference between the macroscopic contact angle measurements and the microscopic data discussed so far is obviously that the former are recorded in ambient brine while the latter were performed in air. It is conceivable that the lack of ability to discriminate between different wetting properties of the asphaltenic layers, arises from the fact that the layers simply look very similar in ambient air but reveal their different composition and response only upon exposure to brine. Hence, we continued to explore the properties of these layers by AFM imaging and spectroscopy, so-called force volume mapping, in ambient brine (using again conventional sharp AFM tips made from silica).

Force-volume mapping experiments can in principle reveal a wealth of information: relative height and stiffness of the layer, and near-contact interactions such as electrostatic, adhesion or hydration forces. However a clean separation of these contributions can be challenging, and to limit the scope of this work we will look only at mechanical properties of the layers and their surface charge, since the former can be extracted from the 'direct contact' region of the force curve and the latter from the long-range region, with no overlap (see Fig. S1). Measurements were performed on mica aged in ASW, ASW-c, and ASW-M^{2+}. The topography and mechanical stiffness images (500 nm scan size) for ASW-M^{2+} are shown in Fig. 8 (measured at pH 6 in ASW and lsASW respectively). Also 50 μm scan size images were measured; these are shown in Supplementary Fig. S6. Median force-distance curves of these measurements give a good impression of the interactions measured; these are shown in Supplementary Fig. S7.

From the topography images it is immediately clear that the structures appear much flatter than for the dry substrates, and no protrusions are visible in the 500 nm images for the standard, and no HCO_3^- samples (although sparse protrusions do exist for all conditions, as shown in the 50 μm images). The substrates aged in ASW-M^{2+} brine also show features, that were not found on dry substrates: protrusions up to 30 nm cover the flatter structures below in a connected network (see Fig. 10A, right column for a 5 μm image showing this network more clearly). Comparing the topography images taken in the ASW and the lsASW ambient brines, none of the samples show much difference.

The calculated interaction stiffness on the different materials (Fig. 8B & 9) show that all samples become softer at low salinity conditions, and that the aforementioned protrusions are much softer than the underlying film. As bare mica is expected to have a much higher stiffness (comparable to that of silica [27,28], which is here assumed to have infinite stiffness for cantilever calibration) which would not alter due to salinity conditions, these results indicate that the entire substrate is covered with a deformable organic film of unknown thickness. The changes in stiffness with salinity could be due to swelling of the organic film, or another form of structural reorganization. Upon drying, the substrates do not return to their original dry topography but do overall

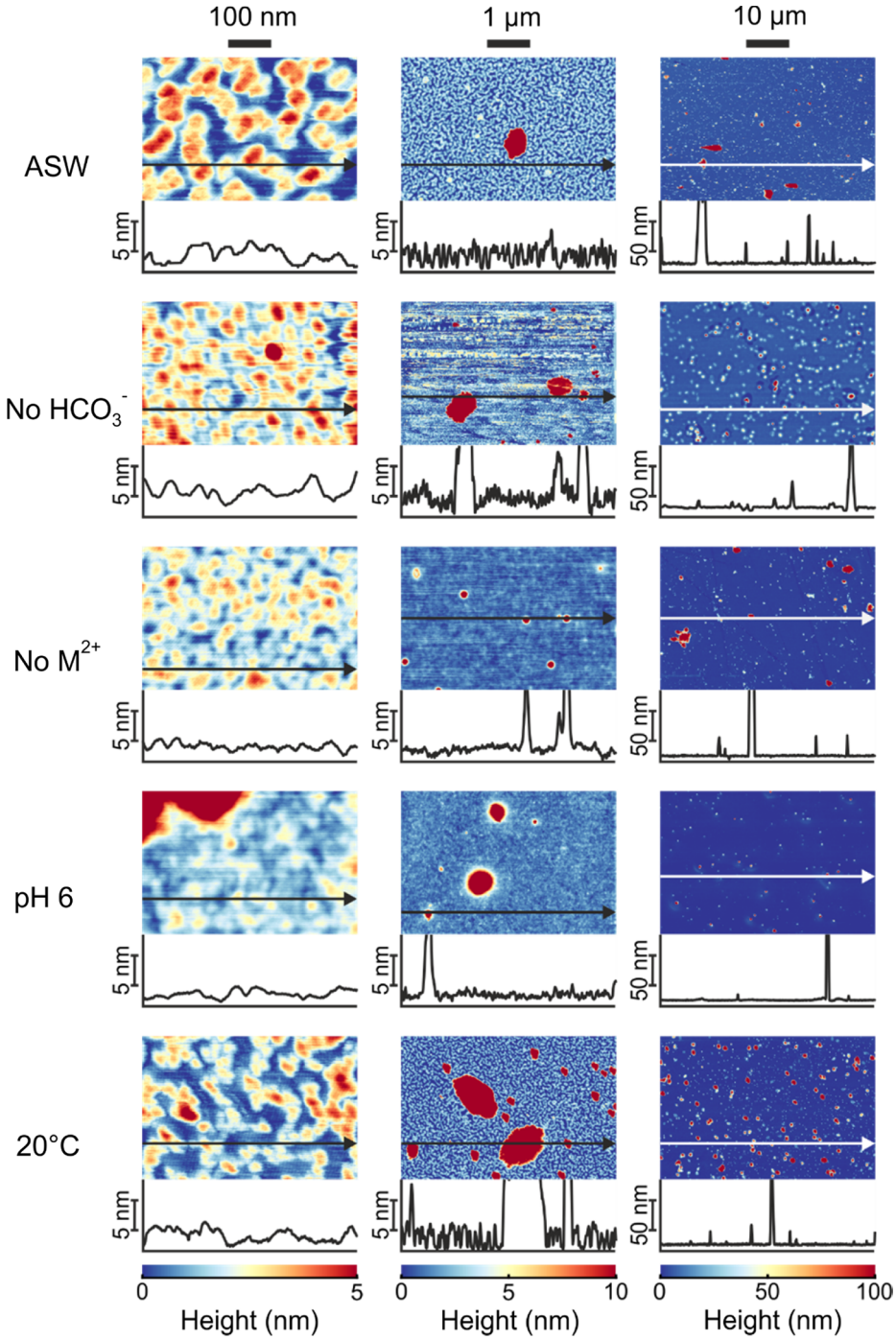

Fig. 5. Substrate topography of dried deposits on mica, obtained using variations on ASW as the aging brine. Representative examples of AFM height images and cross-sections of dried aged mica substrates (ASW and crude oil A at 60 °C) at different lateral scan ranges: 0.5 μm , 5 μm , and 50 μm.

regain some detectable roughness (see Supplementary Fig. S8).

Lastly we also measured the surface charge densities of the substrates, as these are indicative of exposed functional groups. Since the ionic strength felt by the submerged substrates is 26 mM at low salinity conditions, the Debye length is only on the order of 1 nm (see Table 1), which is too small to extract any reliable electric double layer force (see the force curves in Supplementary Fig. S7). Therefore, we also performed the force volume measurements on the same substrates, at 1 mM NaCl and used the exponentially decaying force at tip-sample separations > 5 nm to extract the surface charge (see Fig. S9). Our analysis (see Fig. 10) shows that all samples are predominantly negatively charged, and notably, that the different aging conditions significantly affect the surface charge density. It also shows that surface charge, just like stiffness and chemistry, seems to correlate with topographical structures, indicating a salinity-induced selection of adsorbing (asphaltenic) species during the aging. It turns out that protrusions on the film generally show a more neutral charge, and areas of flat film a stronger, more negative charge.

4. Discussion

Our work complements earlier studies into the effects of mineral aging on wettability in several respects. In several previous works, reservoir core plugs were examined during and after 'long' exposure (up

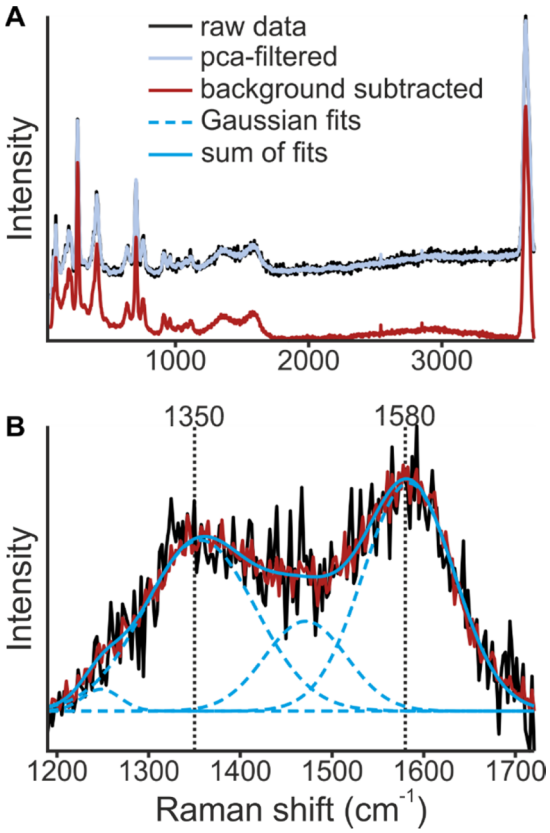

Fig. 6. Raman spectrum captured from an aged mica substrate (ASW and crude oil A, 60 °C, same as in Fig. 7A, ASW): full spectrum + PCA noise-filtering and background subtraction (A), Gaussian fits showing the presence of G- ($\approx$1580 cm^{-1}) and D1-bands ($\approx$1350 cm^{-1}) of noise-filtered background subtracted data, and two additional Gaussian curves needed to obtain a good fit (B).

to a month) to oils and/or brines at elevated temperatures [29–31]. In one case [29] also apparent dynamic contact angles (within the porous medium) were considered in the analysis. We reduced the complexity of the porous reservoir by replacing it with a mica sheet. These perfectly smooth substrates, being somewhat representative for clays adsorbed onto sandstone, facilitated both the measurement of wettability alteration via contact angles, and the microscopic analysis of adsorbed material. The work is in the same spirit as Ref. [17] but more focused on the aspect of aging.

The influence of the aging brine on the wettability of mica involves several stages: the aging brine modifies the mica surface, the altered surface composition changes the adsorption and assembly of components from the crude oil, and the latter finally affects the wettability of the substrate. The overall effect of the aging-brine composition on contact angle alteration was found to be remarkably strong with variations of several tens of degrees (for the same ambient brine). Amazingly, even the direction of the low salinity effect could be reversed, depending on fluid composition and (pH, T) conditions during pre-aging. Meanwhile, using ASW at pH 6 as the aging brine, all 4 crude oils, with rather different chemical makeups, show a similar low salinity effect in ambient ASW at pH 8.8: the oil contact angle increases. While the details of our measurement procedures do certainly not reproduce actual reservoir conditions, the strong responsiveness to the aging brine composition, as observed for several combinations of crude oils and brines nevertheless suggests some general relevance of our observations.

The circumstance that the aging brine influences the wetting behavior indirectly via the adsorbed layer of (at least partially) asphaltenic precipitates, combined with the microscopic characterization of the substrates, allows us to infer qualitatively what might happen during the intermediate steps leading to final wettability alteration. Firstly, the ions in the aging brine must have a significant effect on the mica substrate before the latter gets submerged in the crude oil for further aging. This is not surprising, given the well-known adsorption of ions to mica-brine interfaces [32–35]. A thin aqueous film left behind on the mica will subsequently affect the binding of organic components to the substrate via these ions. Due to the high salinities of the aging brines and the confined nature of the water film, the interactions binding these organic components are likely to be highly ion-specific in nature, e.g. through coordination complexation, as suggested in the MIE scenario [36] and demonstrated e.g. for fatty acid molecules [5]. In analyzing the various aged substrates with AFM we found that these bound organic layers completely cover the substrate, with specific topographic regions correlating with chemical makeup (as found with CRM). It is likely that the ionic content of the aforementioned water film also dictates the architecture of the adsorbed layer: although topographically often similar, chemically and mechanically clear differences were found. While the exact chemical nature of the layers remains unknown, the CRM and surface charge measurements nevertheless indicate that the initial brine content controls the adsorption behavior of the organic compounds. When the organic films are brought in contact with brines, their topography radically changes, likely due to swelling and reorganization. This suggests that some water may penetrate within these organic structures, in agreement with the – at least in some cases – surprisingly hydrophilic character of the organic films.

The surface charge differences of the organic films are key to their effect on wettability and salinity response. The charges are indicative of exposed functional groups such as carboxylates (since we measure mostly negative charges), which can interact with other groups exposed by the crude oil droplet. These surface interactions between adlayer and oil droplet can be either attractive or repulsive, depending on salinity conditions. For example, no effects of changing ambient salinity were found for the samples aged without divalent cations, as oil droplets could not make direct contact with these substrates. These were also the samples that showed networks of protruded areas with a close to neutral charge, suggesting that the absence of divalent cations had promoted the adsorption of uncharged species. Samples that did allow for contact and did show salinity responses were found to be more negatively charged, suggesting the preferential adsorption of compounds with charged groups that facilitate interaction with the oil droplets. This is related to the recent finding of Jackson et al. [37] who reported that the polarity of the oil/water interface, which was shown to depend on the type of crude oil, is crucial for the success of LSWF. We have now shown that this factor not only depends on the oil, but can also be significantly altered by the contents of the connate brine.

Overall, our experiments lead to a perhaps somewhat speculative picture of a highly dynamic and responsive interface where the presence of ions and water has a strong impact on the adsorption of asphaltenes and other polar oil components to the various interfaces, see Fig. 11. The organic layer is first bound to the mica through a brine film present during aging, where the ionic content is an important factor in the preferential adsorption of specific organic compounds. In order to bind these organics, this water film cannot be thicker than a few nm, as this is the typical maximum range of interaction between mineral substrate and asphaltenes [38,39], which is consistent with our silica probe - organic adlayer interaction curves. Upon immersion of the aged substrate into brine, some water seems to penetrate and further alter the film structure. Then a crude oil droplet, also containing charged groups at its interface, is brought in contact with it. Here, again specific ion effects are likely an important factor controlling the oil/substrate interaction. One possible scenario for this would be calcium ion bridging between negatively charged organic groups of the adlayer and the crude oil droplet.

Given the picture of the crude oil-brine-rock interaction process

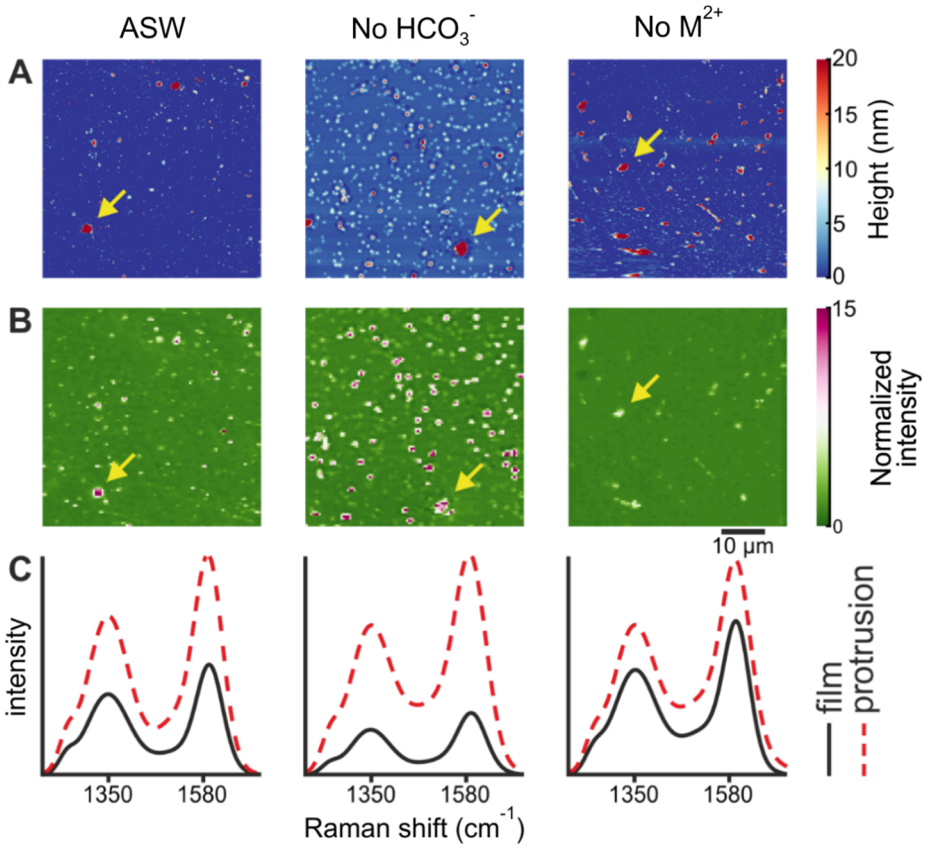

Fig. 7. 50 × 50 µm images of dried aged mica substrates (crude oil A and ASW-based brine, 60 °C): AFM height, 512 × 512 pixels (A), and Raman G- & D-band integrated intensities, normalized to the intensity in the film, 100 × 100 pixels (B). The Gaussian fits (see Fig. 6) to the median G- and D-band spectra of the film (black solid) and protrusions (red dashed) from each map, normalized to the peak intensity of the protrusion G-band, are also shown (C). Arrows in (A) and (B) point to major features for reference.

sketched above, it is likely that the exact outcome of our experiments is affected by our specific choice of sample preparation and aging conditions. Clearly, mimicking aging processes that took millions of years in real reservoirs, by exposing our substrates to brine and crude oil for just a few days, introduces the assumption that the most relevant processes in the reservoir are captured in the lab study. Additionally, one may object that the use of toluene (or any other non-polar solvent) for washing the samples after aging and subsequent drying will affect the sample surface. It is likely that our washing with toluene promoted the desorption of more weakly bound organic molecules. The remaining firmly surface-bound organic layer next to the crude oil drop, as pertinent to our contact angle measurements, may in fact not be a very good representation of reservoir reality. Also the choice of leaving a small amount of aging brine on the mica substrates before immersing them into the crude oil, may have influenced our results. The role of water films in the EOR process has been pointed out by Radke and coworkers [40].

Another aspect about our understanding of the wettability change concerns the composition of the crude oil. Our CRM observations suggest that the adsorption of asphaltenic and acidic molecules is favored, in agreement with the well-known abundance and surface affinity of asphaltenes [41,42]. However, other (e.g. non-aromatic polar) components, which are more difficult to detect with CRM due to the strong background fluorescence, might be involved as well. This is suggested by recent measurements on the salinity dependence of produced oil composition [43]. It is also known that competitive adsorption of crude oil components occurs on rock surfaces; it has been found that initially adsorbed small hydrophilic moieties are subsequently replaced by larger hydrophobic molecules [44,45]. Amongst the larger species, asphaltenes are typically most prominent [46,47] but also resins play a role. In crude oil their contributions may be difficult to dissect, since these different types of molecules can associate in bulk liquid [48]. Comparing (in conjunction) the microscopic self-assembly and macroscopic wettability alterations for different fractions of the same crude oil (keeping all other conditions the same), might shed more light on this aspect.

Yet, the general findings that both i) the properties of the organic adlayer and ii) the responsiveness of this adlayer to the salinity of the ambient brine, depend on the composition of the original connate brine, are expected to prevail even if our simplified experiments are replaced by more elaborate and realistic in situ observations.

5. Conclusions

While it has been known for a long time that the presence of small amounts of brine upon aging mineral surfaces in crude oil is crucial for the subsequent observation of a low salinity response, most attention in recent years has understandably been paid to the effect of the composition of the injection brine on recovery enhancement assuming that existing aging protocols lead to realistic initial conditions for the flooding process. Our results suggest that this assumption may have been oversimplified. Our experiments clearly demonstrate for a variety of crude oils that the properties of organic films deposited onto mineral surfaces upon aging in crude oil strongly depend on the composition of the small amount of brine and ions used to pre-treat the surface before immersion into crude oil. Macroscopic wettability, microscopic

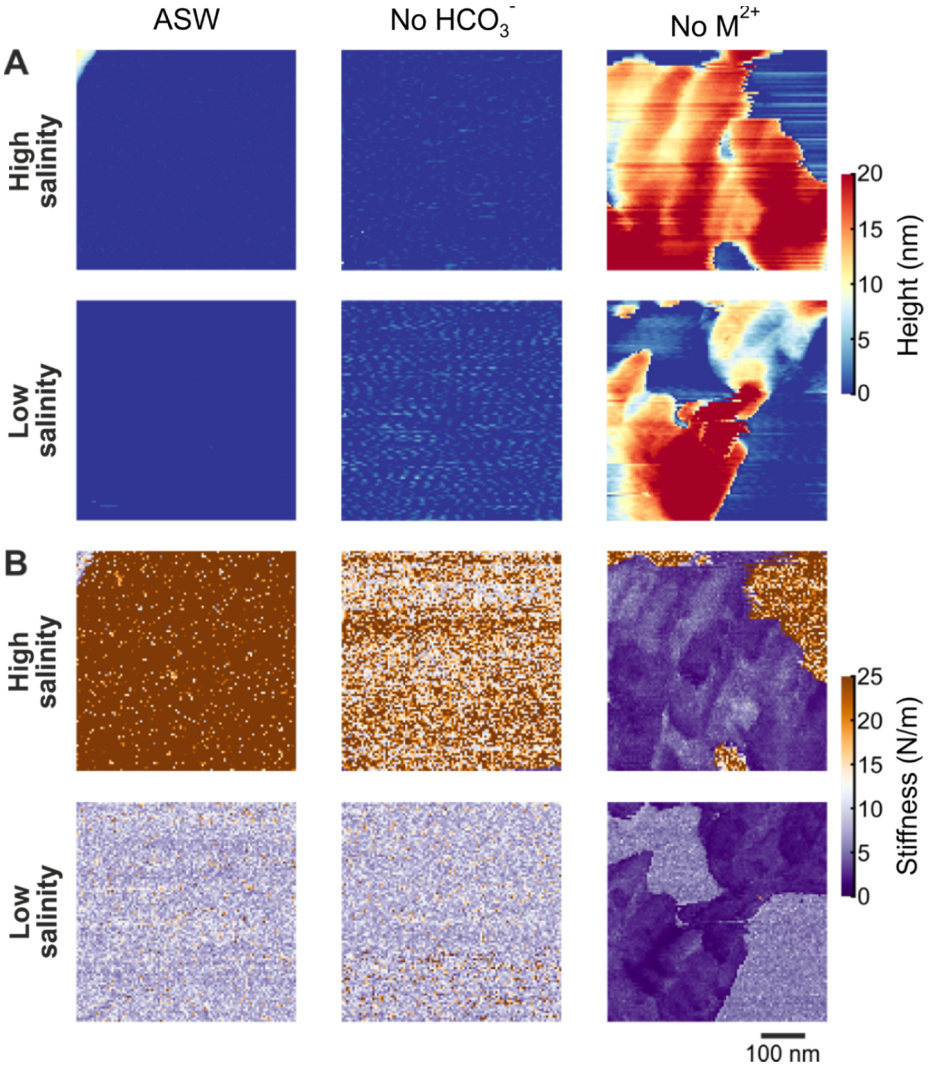

Fig. 8. In-situ force volume AFM measurements at high salinity. 500 × 500 nm images of aged mica substrates (crude oil A and ASW-based brine, 60 °C) submerged in ASW, and lsASW, at pH 6: height (A), and substrate stiffness (B).

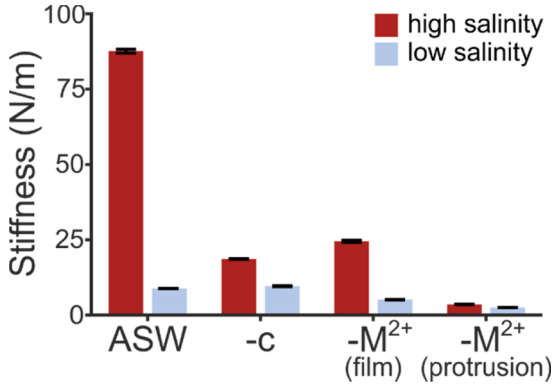

Fig. 9. Mean substrate stiffness and standard errors extracted from 500 × 500 nm force volume maps, measured in ASW and lsASW at pH 6 on mica substrate aged in crude oil A and various ASW-based brines as indicated at 60 °C.

morphology, surface charge, and elasticity of the surface that results after the aging procedure as well as the direction of wettability alteration upon exposure to low salinity water are all affected by the composition of the pre-aging brine. While being far from conclusive regarding specific details, our results nevertheless suggest a picture of a highly dynamic equilibrium between the crude oil and its components that adsorb to the solid surface. The system is apparently highly responsive to small variations of surface properties such as the composition of (presumably) nanometric aqueous films on the surface that seems to selectively trigger the adsorption of specific rather hydrophilic species from the oil. The subtletly of this balance and the difficulties in establishing a correlation between the microscopic properties observed by CRM and in situ AFM spectroscopy suggest that more extended and careful in situ studies at reservoir conditions will be required to establish models that can correctly predict variations of wettability of these soft interfaces in response to LSWF or other methods of EOR. In particular, it seems that more systematic attention should be paid to the crucial effect of aging conditions and procedures.

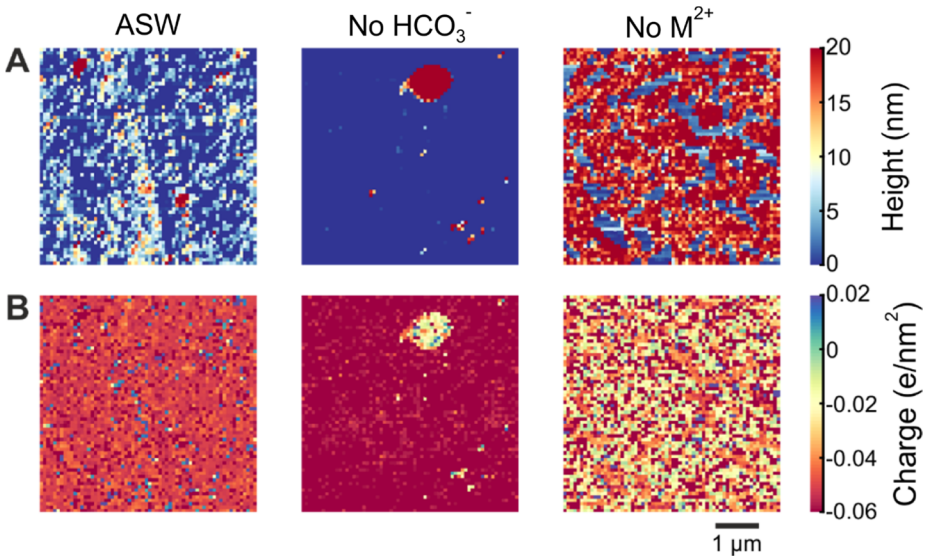

Fig. 10. 5 × 5 µm images extracted from AFM force-volume measurements with a silica probe on aged mica (crude oil A and ASW-based brine, 60 °C), immersed in 1 mM NaCl at 20 °C. These images show that the brine content during aging can significantly affect the density of charged groups of the substrate.

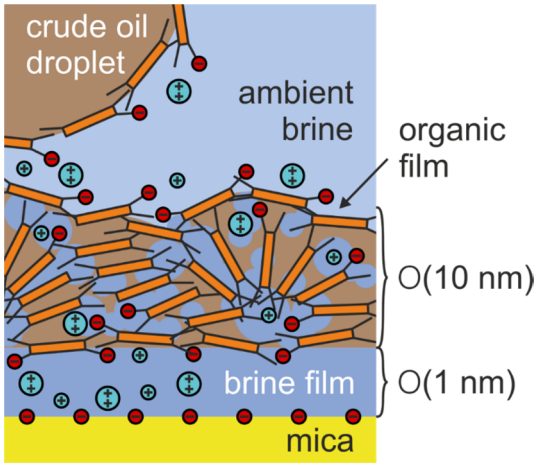

Fig. 11. Schematic representation of a crude oil droplet contacting an aged mica substrate in ambient brine, showing cations interacting with negatively charged groups of asphaltenes and mica.

CRediT authorship contribution statement

M.E.J. Haagh: Investigation, Writing - original draft. **N. Schilderink:** Investigation. **M.H.G. Duits:** Supervision, Writing - original draft. **I. Siretanu:** Supervision. **P. Krawiec:** Conceptualization, Resources. **I.R. Collins:** Conceptualization. **F. Mugele:** Conceptualization, Supervision, Writing - original draft.

Declaration of Competing Interest

The authors declare that they have no known competing financial interests or personal relationships that could have appeared to influence the work reported in this paper.

Acknowledgements

This work is part of the research program Rock-on-a-Chip with project number i40, which is co-financed by the Netherlands Organization for Scientific Research (NWO) and by the Exploratory Research (ExploRe) program of BP plc. BP Exploration Operating Company Limited are thanked for permission to publish this paper. We would like to thank Sachin Nair for the technical support with Raman Spectrometry.

Appendix A. Supplementary data

Supplementary data to this article can be found online at https://doi.org/10.1016/j.fuel.2020.117856.

References

[1] Muggeridge A, et al. Recovery rates, enhanced oil recovery and technological limits. Philos Trans Ser A, Mathe, Phys Eng Sci 2014;372(2006). p. 20120320.
[2] Morrow N, Buckley, J, Improved Oil Recovery by Low-Salinity Waterflooding; 2011.
[3] Morrow NR, et al. Prospects of improved oil recovery related to wettability and brine composition. J Petrol Sci Eng 1998;20(3–4):267–76.
[4] Yu L, Buckley JS. Evolution of wetting alteration by adsorption from crude oil. SPE Form Eval 1997;12(01):5–12.
[5] Mugele F, et al. Ion adsorption-induced wetting transition in oil-water-mineral systems. Sci Rep 2015;5:10519.
[6] Matthiesen J, et al. How naturally adsorbed material on minerals affects low salinity enhanced oil recovery. Energy Fuels 2014;28(8):4849–58.
[7] Tang G-Q, Morrow NR. Influence of brine composition and fines migration on crude oil/brine/rock interactions and oil recovery. J Petrol Sci Eng 1999;24(2–4):99–111.
[8] Jackson M, et al. Evidence, mechanisms and improved understanding of controlled salinity waterflooding part 1: sandstones. Fuel 2016;185:772–93.
[9] Sharma M, Filoco P. Effect of brine salinity and crude-oil properties on oil recovery and residual saturations. SPE J 2000;5(03):293–300.
[10] Liu Q, et al. Wettability alteration by magnesium ion binding in heavy oil/brine/chemical/sand systems—Analysis of electrostatic forces. J Petrol Sci Eng 2007;59(1–2):147–56.
[11] Yang J, et al. Wettability alteration during low-salinity waterflooding and the relevance of divalent ions in this process. Energy Fuels 2016;30(1):72–9.
[12] Shehata AM, Nasr-El-Din HA. Laboratory investigations to determine the effect of connate-water composition on low-salinity waterflooding in sandstone reservoirs. SPE Reservoir Eval Eng 2017;20(01):59–76.
[13] Boek ES, Venturoli M. Lattice-Boltzmann studies of fluid flow in porous media with realistic rock geometries. Comput Math Appl 2010;59(7):2305–14.
[14] Singh K, et al. The role of local instabilities in fluid invasion into permeable media. Sci Rep 2017:7.
[15] AlRatrout A, Blunt MJ, Bijeljic B. Wettability in complex porous materials, the mixed-wet state, and its relationship to surface roughness. PNAS 2018;115(36):8901–6.
[16] Buckley JS, Lord DL. Wettability and morphology of mica surfaces after exposure to crude oil. J Petrol Sci Eng 2003;39(3–4):261–73.
[17] Kumar K, Dao E, Mohanty KK. AFM study of mineral wettability with reservoir oils. J Colloid Interface Sci 2005;289(1):206–17.
[18] Kumar N, et al. Characterization of the surface charge distribution on kaolinite particles using high resolution atomic force microscopy. Geochim Cosmochim Acta 2016;175:100–12.
[19] Ebeling D, Van den Ende D, Mugele F. Electrostatic interaction forces in aqueous salt solutions of variable concentration and valency. Nanotechnology 2011;22(30):305706.

[20] Israelachvili JN. Intermolecular and surface forces. revised third ed. Academic press; 2011.
[21] Zhang Z-M, Chen S, Liang Y-Z. Baseline correction using adaptive iteratively reweighted penalized least squares. Analyst 2010;135(5):1138–46.
[22] Shi L, et al. A pH-resolved view of the low salinity effect in sandstone reservoirs. Energy Fuels 2016;30(7):5346–54.
[23] Joonaki E, et al. Water versus Asphaltenes; liquid-liquid and solid-liquid molecular interactions unravel the mechanisms behind an improved oil recovery methodology. Sci Rep 2019;9(1):11369.
[24] Cadena-Nava RD, Cosultchi A, Ruiz-Garcia J. Asphaltene behavior at interfaces. Energy Fuels 2007;21(4):2129–37.
[25] Nair S, et al. Algorithm-improved high speed and non-invasive confocal Raman imaging of two-dimensional materials. Natl Sci Rev 2019.
[26] Abdallah WA, Yang Y. Raman spectrum of asphaltene. Energy Fuels 2012;26(11):6888–96.
[27] Engineering ToolBox: Young's Modulus - Tensile and Yield Strength for common Materials. 2003 [cited 2019 30/12/2019]; Available from: https://www.engineeringtoolbox.com/young-modulus-d_417.html.
[28] Teich-McGoldrick SL, Greathouse JA, Cygan RT. Molecular dynamics simulations of structural and mechanical properties of muscovite: pressure and temperature effects. J Phys Chem C 2012;116(28):15099–107.
[29] Zhou XM, Morrow NR, Ma SX. Interrelationship of wettability, initial water saturation, aging time, and oil recovery by spontaneous imbibition and waterflooding. SPE J 2000;5(2):199–207.
[30] Ferno MA, et al. Dynamic laboratory wettability alteration. Energy Fuels 2010;24(7):3950–8.
[31] Graue A, et al. Systematic wettability alteration by aging sandstone and carbonate rock in crude oil. J Petrol Sci Eng 1999;24(2–4):85–97.
[32] Israelachvili JN, Pashley RM. Measurement of the hydrophobic interaction between 2 hydrophobic surfaces in aqueous-electrolyte solutions. J Colloid Interface Sci 1984;98(2):500–14.
[33] Pashley RM, Israelachvili JN. DLVO and hydration forces between mica surfaces in MG-2+, CA-2+, SR-2+, AND BA-2+ chloride solutions. J Colloid Interface Sci 1984;97(2):446–55.
[34] Zhao CL, et al. Extracting local surface charges and charge regulation behavior from atomic force microscopy measurements at heterogeneous solid-electrolyte interfaces. Nanoscale 2015;7(39):16298–311.
[35] Siretanu I, et al. Direct observation of ionic structure at solid-liquid interfaces: a deep look into the Stern Layer. Sci Rep 2014;4:4956.
[36] Alvarez G, et al. Heavy oil-water interfacial properties and emulsion stability: influence of dilution. Energy Fuels 2009;23(1):294–9.
[37] Jackson MD, Vinogradov J. Impact of wettability on laboratory measurements of streaming potential in carbonates. Colloids Surf, A 2012;393:86–95.
[38] Hu X, et al. Asphaltene adsorption from toluene onto silica through thin water layers. Langmuir 2019;35(2):428–34.
[39] Gonzalez V, Taylor SE. Asphaltene adsorption on quartz sand in the presence of preadsorbed water. J Colloid Interface Sci 2016;480:137–45.
[40] Freer EM, Svitova T, Radke CJ. The role of interfacial rheology in reservoir mixed wettability. J Petr Sci Eng 2003;39:137–58.
[41] Buckley JS, et al. Asphaltenes and crude oil wetting-the effect of oil composition. SPE J 1997;2(02):107–19.
[42] Buckley JS, Wang J. Crude oil and asphaltene characterization for prediction of wetting alteration. J Petrol Sci Eng 2002;33(1–3):195–202.
[43] Collins IR, et al. Effect of low salinity waterflooding on the chemistry of the produced crude oil. SPE Improved Oil Recovery Conference. Tulsa, Oklahoma, USA: Society of Petroleum Engineers; 2018. p. 17.
[44] Bennett B, et al. Wettability alteration in petroleum systems: the role of polar nonhydrocarbons. Pet Geosci 2004;10(3):271–7.
[45] Li XG, et al. Understanding desorption of oil fractions from mineral surfaces. Fuel 2018;232:257–66.
[46] Adams JJ. Asphaltene adsorption, a literature review. Energy Fuels 2014;28(5):2831–56.
[47] Li MY, et al. Interfacial film properties of asphaltenes and resins. Fuel 2002;81(14):1847–53.
[48] Ekholm P, et al. A quartz crystal microbalance study of the adsorption of asphaltenes and resins onto a hydrophilic surface. J Colloid Interface Sci 2002;247(2):342–50.